NANO LETTERS

Letter

pubs.acs.org/NanoLett

Room-Temperature Giant Stark Effect of Single Photon Emitter in van der Waals Material

Yang Xia,[†,§] Quanwei Li,[†,§] Jeongmin Kim,[†] Wei Bao,[†] Cheng Gong,[†] Sui Yang,[†] Yuan Wang,[†] and Xiang Zhang*[,†,‡]

[†]Nanoscale Science and Engineering Center (NSEC), University of California, 3112 Etcheverry Hall, Berkeley, California 94720, United States

[‡]Faculty of Sciences and Engineering, University of Hong Kong, Pokfulam, Hong Kong

Supporting Information

ABSTRACT: Single photon emitters (SPEs) are critical building blocks needed for quantum science and technology. For practical applications, room-temperature solid-state platforms are critically demanded. To scale up quantum information processing using, for example, wavelength division multiplexing quantum key distribution, a large tuning range beyond emission line width of single photon energy is required. Stark effect can tune the single photon energy by an electric field. However, it has been achieved only at cryogenic temperature to pursue a shift larger than emission line width. A large stark tuning beyond emission line width at room temperature still remains elusive. Here we report the first room-temperature Stark effect of SPEs with a giant Stark shift of single photon energy up to 43 meV/(V/nm), largest among all previous color center emitters. Such a giant Stark shift is 4-fold larger than its line width at room temperature, demonstrated by exploiting hBN color centers. Moreover, the intrinsic broken symmetries are determined via angle-resolved Stark effect, for the first time, by the orientation of the electric permanent dipole moment in the solid-state SPE, which is unachievable in traditional optical polarization measurement. The remarkable Stark shift discovered here and the significant advance in understanding its atomic structure pave a way toward the scalable solid-state on-chip quantum communication and computation at room temperature.

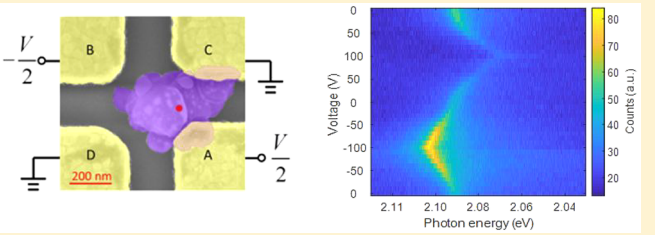

KEYWORDS: *Stark effect, single photon emitter, hexagonal boron nitride, color center, symmetry breaking, permanent electric dipole moment*

Over the last two decades owing to their exceptional electronic and optical properties, van der Waals (vdW) materials, ranging from semi-metallic graphene[1] and semiconducting transition-metal dichalcogenides[2] to insulating hexagonal boron nitride (hBN), have enabled remarkable scientific and technological breakthroughs. Both the single materials and the heterostructures have been exploited to demonstrate appealing device applications,[3] such as light-emitting diodes,[4] lasers,[5] and optical modulators.[6] While most cases deal with classical information, only a few studies have been reported in the quantum regime at liquid helium temperature.[7−12] Recently, color centers in hBN have emerged as superb room-temperature solid-state single photon emitters (SPEs),[13] which opens up the possibilities of utilizing vdW materials as a platform for room-temperature solid-state quantum information systems.[14−16] They are capable of working at room temperature and are among the brightest SPEs due to their high internal quantum efficiency. Moreover, high-efficiency photon extraction can be greatly facilitated by their intrinsic layered material structure.[13] Consequently, millions of linearly polarized photons per second can be easily detected without additional photon extraction structures. Furthermore, their facile integration with photonic and electrical components is highly preferred for integrated on-chip quantum information systems.[2,3,17]

One major challenge for all solid-state SPEs is the random variation of emission energy caused by the inhomogeneity in local environment. Such variation breaks the indistinguishability of single photons from multiple emitters, which is critically required for large-scale quantum computation, such as universal linear optics[18] and boson sampling.[19] The randomness also prevents scaling up the room-temperature quantum communication systems from using wavelength-division multiplexing (WDM) where indistinguishability is not required, due to the stringent requirement on the precision of photon energy placed by the narrow-band optics.[3] Stark effect, which describes the shift of spectra lines by an external electric field (Figure 1c), can precisely control SPE photon energy and be facilely integrated into quantum systems,[20] advantageous over other tuning methods such as temperature,[21] strain,[22,23] and magnetic field.[24] It has been used to tune the emission

Received: June 28, 2019
Revised: September 6, 2019
Published: September 13, 2019

DOI: 10.1021/acs.nanolett.9b02640
Nano Lett. XXXX, XXX, XXX−XXX

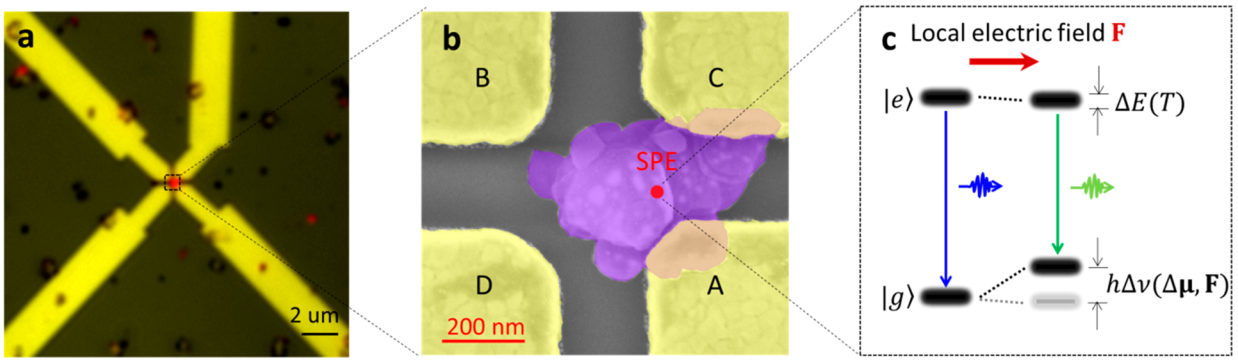

Figure 1. Device and physics of the Stark effect in hBN SPE at room temperature. (a) Two-channel optical image of the fabricated four-electrode device (yellow, bright-field image of the gold electrodes; red, PL image of the hBN SPE). (b) Zoom-in pseudocolor SEM image of the same device. The hBN nanoflake (purple) hosts the SPE (red dot) whose position is found from a localization image analysis of (a) (see Figure S1 for details). A, B, C and D (yellow) denote the four gold electrodes where voltages are applied to generate external electric fields. (c) Illustration of the Stark effect of the SPE (represented by a two-level system) with an optical transition from the excited state $|e\rangle$ to the ground state $|g\rangle$. The emitted photon energy is tuned via shifting the electronic levels by a local electric field **F**. At room temperature, the electronic levels and thus the emitted photon energy are broadened (characterized by $\Delta E(T)$) due to electron−phonon scattering, which sets the minimum Stark shift needed for practical use.

energy of quantum dots,[20] SPEs in layered WSe_2,[25] atomic emitters such as NV centers and SiV centers in diamond,[26−29] and organic dye molecules.[30] However, because either the emitters only produce single photons at low temperature or the effect was too weak to observe at room temperature, all the previously demonstrated Stark shifts in these traditional SPEs were at liquid helium temperature, placing significant challenges for practical quantum applications.

In this paper, we report the first room-temperature Stark effect of SPEs up to 43 meV/(V/nm), discovered in hBN color centers with an in-plane nanoscale electrode design. Moreover, we develop a rotating field method to resolve the angular dependence of the Stark effect to determine the underlying symmetry of the color center. With this method, we directly observe, for the first time, a dipolar pattern of the Stark shift that is well aligned with the optical polarization. This dipolar pattern unambiguously reveals an electric permanent dipole moment which proves the breaking of inversion and rotation symmetries at the hBN SPE. The discovered remarkably giant room-temperature Stark effect and the significant advance in understanding its atomic structure could enable new possibilities of quantum information technologies, such as WDM and indistinguishable single photon sources, at room temperature.

Results and Discussion. To achieve large Stark shift of our hBN SPEs and to fully characterize its dependence on the amplitude and orientation of the local electric fields, we design the nanoscale four-electrode device (Figure 1). SPEs in multilayer hBN nanoflakes are chosen due to their much better optical performance compared to those in monolayers.[13] Multiple electrodes are carefully designed to surround the SPEs such that we can control not only the amplitude but also the direction of the electric field, in contrast to the experiments using vertical electrodes where the electric field is limited in a fixed direction.[31−34] We develop a down-scaled four-electrode device with gaps as small as 200 and 400 nm between the adjacent and diagonal electrodes, respectively. In this case, it can achieve unprecedented large electric field on the order of 0.1 V/nm, orders of magnitude higher than previous reports using similar in-plane electrode design.[27,35] Figure 1a,b shows microscope images of the fabricated four-electrode device. We locate the SPE on the hBN flake by a localization analysis of its photoluminescence (PL) profile with respect to the electrodes (see Figure S1 for details).

The high-quality single-photon emission from the hBN color center is verified by PL spectroscopy at room temperature before applying external electric fields (Figure 2a). The majority of its PL emission is attributed to the zero-phonon line (ZPL) at 2.088 eV. The narrow full width at half-maximum (~7 meV) provides evidence as a high-quality emitter. Two small phonon sidebands (PSBs) are observed at 1.921 eV (PSB1) and 1.753 eV (PSB2), with the frequency difference of ~1370 cm^{-1} corresponding to the E_{2g} phonon of hBN.[36] The well-resolved doublet at PSB1 is a typical feature for hBN nanoflake.[15−17] A few tiny peaks are visible that might result from the PL emission of other color centers in the collected region. The emission of the hBN SPE is linearly polarized (blue circles and curve in Figure 3b), which fits well to a cosine-squared function with a visibility of 0.72. Many SPEs are characterized under the identical pump laser polarization, and the detected photons are linearly polarized in various directions, thus the polarization observed here is specific to the SPE and not due to optical excitation. We measure the second-order coherence function ($g^{(2)}$) after device fabrication using a Hanbury Brown and Twiss (HBT) setup, from which single photon emission is confirmed by a raw antibunching dip of $g^{(2)}(0) = 0.45$ (Figure 2a inset). By fitting the $g^{(2)}$ data to a single exponential decay function, we estimate the lifetime of our SPE to be 4.2 ns.

After characterizing and confirming the SPE optical properties, we apply voltages within ±100 V between the electrodes A and B (Figure 2b inset) to study the Stark effect. PL emission spectra are collected at each voltage. Figure 2b plots the ZPL PL intensity map as a function of photon energy and applied voltage. A huge Stark shift of 31 meV is clearly observed which is 4-fold larger than its room-temperature line width (~7 meV). Based on our calculation, such voltage generates a local electric field ~0.36 V/nm, which indicates a large effect of 43 meV/(V/nm). To further analyze the effect, we extract the ZPL peak position as a function of applied voltage in Figure 2c. The Stark shift is approximately linear to the applied voltage with a tuning efficiency of 137 μeV/V and reverses sign at opposite electric field, which suggests a nonzero electric permanent dipole moment at the color

DOI: 10.1021/acs.nanolett.9b02640
Nano Lett. XXXX, XXX, XXX−XXX

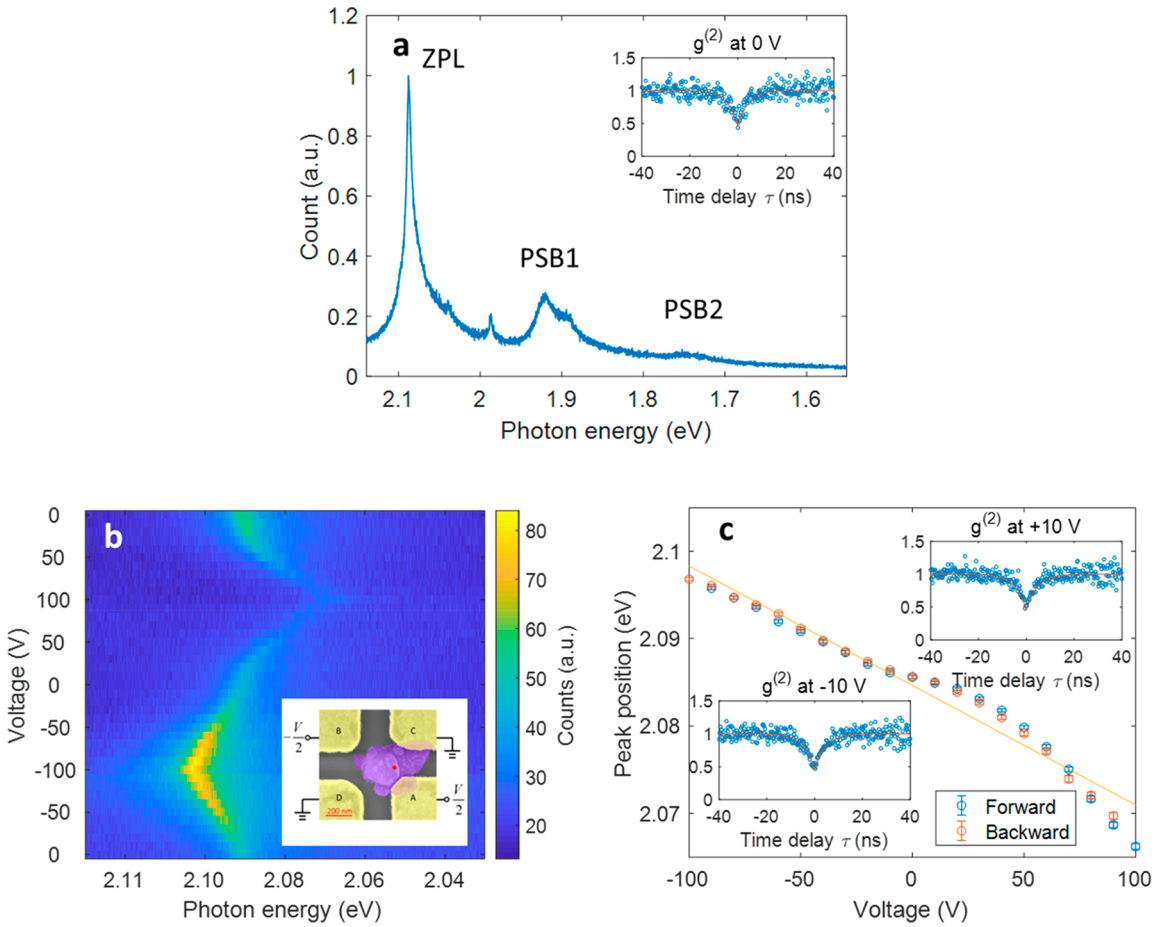

Figure 2. Observation of room-temperature giant Stark effect in hBN SPE. (a) PL spectrum of the SPE at 300 K without applying electric field. It shows a dominating ZPL at 2.088 eV with 7 meV full width at half-maximum (fwhm) and two phonon sidebands (PSB1 and PSB2). The small peak at 1.988 eV stems from another emitter nearby. Inset: The measured (circles) and fitted (red curve) second-order coherence function $g^{(2)}$ of the SPE PL after device fabrication. The $g^{(2)}(0)$ of 0.45 demonstrates the single-photon nature. The measurement data are well fitted by a single exponential decay with a lifetime of 4.2 ns. (b) ZPL spectra of the hBN SPE as a function of voltage applied to electrodes A and B (inset) with equal magnitude at opposite signs. The achieved Stark shift is up to 31 meV, 4 times greater than its own room-temperature line width. A gradual decrease in its intensity is noted when voltage changes from −100 to 100 V (Figure S2a), which is possibly due to the change of coupling to dark state as reported previously in diamond NV center.[28] (c) Voltage controlled ZPL energy extracted from emission spectra fitting from (b). The blue and orange dots correspond to experiment data obtained during the forward and backward sweeping of voltages, respectively. Error bar, 95% confidence interval of the fitting. A tuning efficiency of 137 μeV/V is obtained by linear regression (yellow solid line). Insets show $g^{(2)}$ of the device measured at ±10 V, certifying that the single photon emission remains under external electric fields. The spectra and $g^{(2)}$ are measured under the excitations of continuous-wave 473 and 532 nm lasers, respectively. The acquisition time for $g^{(2)}$ is 10 s. The excitation intensity is 100 μW/μm^2 for all measurements. All the Stark effect data are measured in vacuum, while $g^{(2)}$ is done in ambient air.

center.[27] The slight deviation from linearity is possibly due to the light induced ionization in nearby nonemitting defects.[27] The line width of the emission does not show clear dependence on the applied electric field, consistent with previous reports on color center SPEs[35] (Figure S2b). The repeatability and stability of such room-temperature giant Stark effect are further characterized in multiple emitters (Figures S3−S5). A similar tuning range is also obtained at 80 K (Figure S6), which also confirms the giant Stark effect is intrinsic to the emitters rather than a temperature-induced effect and is consistent with a previous report.[31]

The underlying symmetry of the atomic structure can be further revealed by the Stark shift that depends not only on the magnitude of the applied field but also its orientation.[37] We develop here a rotating field method to probe electric permanent dipole of the hBN SPE by characterizing the angular dependence of the Stark effect. With a fixed local electric field magnitude of 0.08 V/nm, the ZPL is 1.13 meV red (1.32 meV blue) shifted when the applied field points to 140° (320°), while the shift with the electric field along 230° is negligible. The Stark shift $h\Delta\nu$ as a function of the angle θ of the local field $\mathbf{F}$ is well-fitted with the electric permanent dipole moment model (Figure 3b) based on perturbation theory to the first order:

$$h\Delta\nu = -\Delta\boldsymbol{\mu} \times \mathbf{F} = -|\Delta\boldsymbol{\mu}||\mathbf{F}|\cos(\phi - \theta) \quad (1)$$

where $\Delta\boldsymbol{\mu}$ and ϕ denote the dipole moment responsible for the Stark effect and its orientation angle, respectively. Such a result further justifies that the Stark effect is dominated by an electric permanent dipolar term. From the fitting, we estimate the magnitude of the dipole is $|\Delta\boldsymbol{\mu}| = 0.65 \pm 0.04$ D, where 1 D = 3.33×10^{-30} Cm, which is on the same order as the NV center in a diamond.[26] The discovered electric permanent dipole moment corresponds to the asymmetric charge distribution at the hBN SPE, which will facilitate the future study of the atomic structure and electronic levels of the color center. In

DOI: 10.1021/acs.nanolett.9b02640
Nano Lett. XXXX, XXX, XXX−XXX

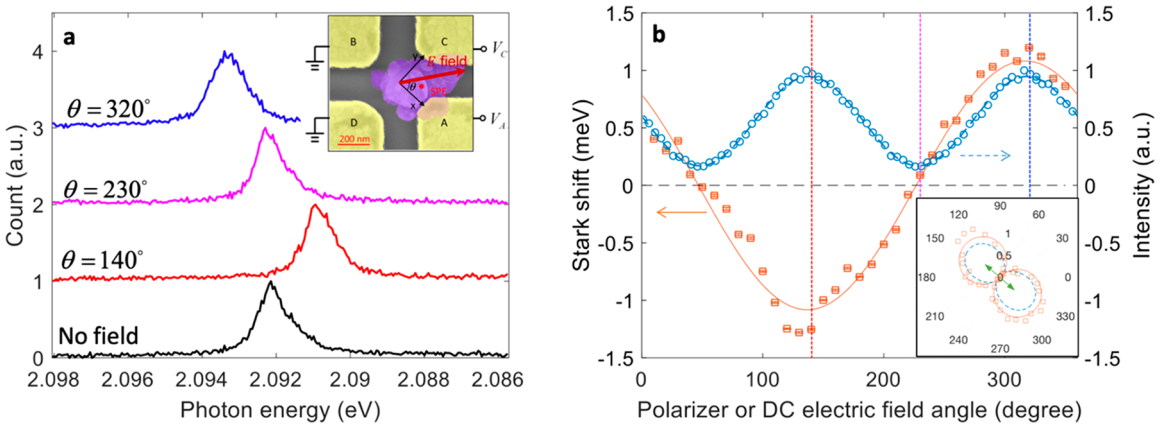

Figure 3. Angle-resolved Stark effect of hBN SPE and the discovered symmetry breaking. (a) ZPL spectra of hBN SPE recorded with electric fields applied in various orientations θ (defined in the inset) with a fixed magnitude ($\mathbf{F}$ = 0.08 V/nm). Such electric fields are generated by applying voltages to electrodes A and C (inset, see Methods for details). The zero-field spectrum is plotted for comparison. When we apply an electric field along 140° (320°) directions, a 1.32 meV red (1.13 meV blue) shift of ZPL is observed. On the contrary, the electrical field along 230° does not cause noticeable change in the ZPL spectrum. (b) Angle-resolved Stark shift (orange color, left y axis) and optical polarization data (blue color, right y axis). The x axis corresponds to the orientation angle of the applied electric field and that of the polarizer in front of the photodetector, respectively. The orange squares (blue circles) are the measured Stark shift (ZPL intensity) of the single photons, and the solid orange line (dashed blue line) is the fitting curve according to the electric permanent dipole model in eq 1 (to the linearly polarized emission in cosine-squared function). The unveiled electric permanent dipole moment uncovers the broken inversion and rotation symmetries at the atomic color center. The electric permanent dipole moment aligns well with the emission polarization. The inset shows the same data in polar coordinates. The excitation laser is polarized along the green arrow direction. Three vertical dashed lines in the main panel (blue, magenta and red) correspond to the three spectra in (a). The photon energies in (b) are obtained by fitting the ZPLs with the Lorentzian line shape. The error bars from fitting are smaller than 0.03 meV. The Stark shift is measured at 80 K to reduce ZPL fitting uncertainty at small shifts, taking advantage of the narrow line width at low temperature. The optical polarization is measured at room temperature without applying voltage. As shown in Figure S7, the emission polarization only exhibits a small change even with large Stark shift.

contrast, the linear polarization of emitted photons characterized in earlier reports is determined only by the optical transition dipole and features cosine-squared angular dependence, which omits the information for inversion symmetry of atomic structure (see Methods). We clarify such a distinctive difference in Figure 3b (blue circles). It should be noted that the direction for maximum Stark shift is coincident with that of the emission polarization (Figure 3b inset), which corresponds to the intersection of the mirror symmetry plane of the color center and the hBN atomic layer plane.

We emphasize that the key to observe the room-temperature giant Stark shift is a combined effort of several crucial factors. First, the large band gap of hBN crystal and low phonon scattering make a superb room-temperate SPE. Second, the layered structure of hBN likely leads to an in-plane dipole moment,[13] such that an applied in-plane electric field can be well aligned with the dipole orientation. Third, a nanometer-sized four-electrode system not only allows us to achieve the control electric field orientation but also reach unprecedented in-plane field strength on the order of 0.1 V/nm.

For the first time, we report the room-temperature Stark effect of an SPE up to 43 meV/(V/nm) in hBN color center with a tuning range exceeding 4 times its line width. With developing a rotating field method, we uncover the intrinsic broken symmetries of color centers in hBN through angle-resolved Stark effect. Our results provide a fundamental knowledge for the understanding and applications of color centers in vdW materials and open a new route toward scalable solid-state quantum information systems at room temperature.

Methods. *Device Fabrication.* The hBN nanoflakes are purchased from the Graphene Supermarket, in the form of a liquid suspension, and drop-cast on a silicon substrate (resistivity 1−50 Ω·cm) with ∼280 nm thermal oxide on top. The samples are then annealed at 1000 C for 30 min in an Ar/H_2 environment followed by slow cooling down. Individual SPEs are found by fluorescence microscopy and characterized by PL emission spectroscopy, polarization analysis, and $g^{(2)}$ measurement. Electron beam lithography is used to define the electrode pattern around the located SPEs. The electrodes are made of 5 nm Ti and 100 nm Au deposited by electron beam evaporation.

Rotating Field Method. When we apply an electric field via multiple electrodes, the total external field can be considered as linear combination of the fields generated by individual electrodes. In our experiment, two voltage signals are applied to electrodes A and C (Figure 3b inset), while the other two electrodes and substrate are grounded. From linear combination, we have the equation below:

$$\begin{bmatrix} E_x \\ E_y \end{bmatrix} = \mathbf{K} \begin{bmatrix} V_A \\ V_C \end{bmatrix}$$

where E_x and E_y are the x and y components of external electric field at the SPE location, $\mathbf{K}$ is a 2 × 2 matrix, and V_A and V_C are the voltages applied to electrodes A and C, respectively. Matrix $\mathbf{K}$ is obtained from three-dimensional FEM simulation (COMSOL). The simulated geometry is extracted from the real device. In order to obtain the first column of $\mathbf{K}$, we assign V_A = 1 V and ground electrodes B, C, D. The obtained E_x and E_y form the first column of $\mathbf{K}$, and the second column can be calculated similarly.

In order to generate a local field with specific amplitude F_0 and direction θ, we consider the following equation:

DOI: 10.1021/acs.nanolett.9b02640
Nano Lett. XXXX, XXX, XXX−XXX

$$\begin{bmatrix} E_x \\ E_y \end{bmatrix} = \frac{F_0}{L}\begin{bmatrix} \cos(\theta) \\ \sin(\theta) \end{bmatrix}$$

Here we follow previous works and use the Lorentz approximation to calculate the local field from the external field. $L = (\varepsilon_r + 2)/3$ is the Lorentz factor. The relative permittivity ε_r is taken from ref 36. Combining the two equations above gives

$$\begin{bmatrix} V_A \\ V_C \end{bmatrix} = \frac{F_0}{L}\mathbf{K}^{-1}\begin{bmatrix} \cos(\theta) \\ \sin(\theta) \end{bmatrix}$$

Structure Information from Discovered Electric Permanent Dipole Moments. The electric permanent dipole moments correspond to the charge distributions of the electronic states of the SPEs. It can be calculated for the ground and excited states of an SPE as

$$\boldsymbol{\mu}_{g,e} = \int \psi_{g,e}^{*} e\mathbf{r}\psi_{g,e} dr^3$$

where ψ is the wave function of electronic states, and the subscripts g and e correspond to ground and excited states, respectively. Such dipole moments contribute to Stark shift through $\Delta\boldsymbol{\mu} = \boldsymbol{\mu}_e - \boldsymbol{\mu}_g$ (eq 1). A nonvanishing $\Delta\boldsymbol{\mu}$ indicates nonzero $\boldsymbol{\mu}_e$ and/or $\boldsymbol{\mu}_g$, which must result from non-inversion symmetric probability densities of electrons $|\psi_e|^2$ and/or $|\psi_g|^2$ as well as atomic structure.

On the contrary, the optical polarization is determined by optical transition dipole moment $\boldsymbol{\mu}_{e\to g} = \int \psi_g^{*} e\mathbf{r}\psi_e dr^3$, which emits an optical wave with electric field parallel to the dipole, along the directions normal to it. After polarizer, the detected optical intensity has a squared-cosine dependence $I(\theta) = I_0 \cos^2(\theta)$ on polarization angle θ, which returns itself after $\theta \to \theta + 180°$. As such measurement is always inversion symmetric, it cannot tell whether inversion symmetry breaks or not at the emitter.

■ ASSOCIATED CONTENT

Supporting Information

The Supporting Information is available free of charge on the ACS Publications website at DOI: 10.1021/acs.nanolett.9b02640.

Additional experimental details and data (PDF)

■ AUTHOR INFORMATION

Corresponding Author

*E-mail: xiang@berkeley.edu.

ORCID

Xiang Zhang: 0000-0002-3272-894X

Author Contributions

§These authors contributed equally to this work. Y.X., Q.L., and X.Z. conceived the idea and initiated the project. Y.X. designed and fabricated the devices. W.B. assisted the fabrication. Q.L. prepared the emitters and performed optical measurements. J.K. performed emitter localization microscopy. Y.X. and Q.L. measured the Stark effect and analyzed data. C.G. assisted with the data analysis. Y.X. and Q.L. prepared the manuscript. X.Z., Y.W., and S.Y. supervised the project. All authors contributed to discussions and manuscript revision.

Notes

The authors declare no competing financial interest.

■ ACKNOWLEDGMENTS

This work was supported by the Office of Naval Research Multidisciplinary University Research Initiative program under grant no. N00014-13-1-0678, the National Science Foundation (NSF) under grant 1753380, and Samsung Electronics.

■ REFERENCES

(1) Geim, A. K.; Novoselov, K. S. The Rise of Graphene. *Nat. Mater.* **2007**, *6* (3), 183.

(2) Xia, F.; Wang, H.; Xiao, D.; Dubey, M.; Ramasubramaniam, A. Two-Dimensional Material Nanophotonics. *Nat. Photonics* **2014**, *8* (12), 899−907.

(3) Geim, A. K.; Grigorieva, I. V. Van Der Waals Heterostructures. *Nature* **2013**, *499* (7459), 419−425.

(4) Sundaram, R. S.; Engel, M.; Lombardo, A.; Krupke, R.; Ferrari, A. C.; Avouris, Ph.; Steiner, M. Electroluminescence in Single Layer MoS2. *Nano Lett.* **2013**, *13* (4), 1416−1421.

(5) Ye, Y.; Zhu, H.; Zhang, X.; Chen, X.; Ni, X.; Lu, X.; Wang, Y.; Wong, Z. J. Monolayer Excitonic Laser. *Nat. Photonics* **2015**, *9* (11), 733.

(6) Liu, M.; Geng, B.; Ulin-Avila, E.; Wang, F.; Ju, L.; Zentgraf, T.; Zhang, X.; Yin, X. A Graphene-Based Broadband Optical Modulator. *Nature* **2011**, *474* (7349), 64.

(7) Koperski, M.; Nogajewski, K.; Arora, A.; Cherkez, V.; Mallet, P.; Veuillen, J.-Y.; Marcus, J.; Kossacki, P.; Potemski, M. Single Photon Emitters in Exfoliated WSe2 Structures. *Nat. Nanotechnol.* **2015**, *10* (6), 503−506.

(8) Tonndorf, P.; Schmidt, R.; Schneider, R.; Kern, J.; Buscema, M.; Steele, G. A.; Castellanos-Gomez, A.; van der Zant, H. S. J.; Michaelis de Vasconcellos, S.; Bratschitsch, R. Single-Photon Emission from Localized Excitons in an Atomically Thin Semiconductor. *Optica* **2015**, *2* (4), 347.

(9) Srivastava, A.; Sidler, M.; Allain, A. V.; Lembke, D. S.; Kis, A.; Imamoğlu, A. Optically Active Quantum Dots in Monolayer WSe2. *Nat. Nanotechnol.* **2015**, *10* (6), 491−496.

(10) He, Y.-M.; Clark, G.; Schaibley, J. R.; He, Y.; Chen, M.-C.; Wei, Y.-J.; Ding, X.; Zhang, Q.; Yao, W.; Xu, X.; et al. Single Quantum Emitters in Monolayer Semiconductors. *Nat. Nanotechnol.* **2015**, *10* (6), 497−502.

(11) Chakraborty, C.; Kinnischtzke, L.; Goodfellow, K. M.; Beams, R.; Vamivakas, A. N. Voltage-Controlled Quantum Light from an Atomically Thin Semiconductor. *Nat. Nanotechnol.* **2015**, *10* (6), 507−511.

(12) Palacios-Berraquero, C.; Barbone, M.; Kara, D. M.; Chen, X.; Goykhman, I.; Yoon, D.; Ott, A. K.; Beitner, J.; Watanabe, K.; Taniguchi, T.; et al. Atomically Thin Quantum Light-Emitting Diodes. *Nat. Commun.* **2016**, *7*, ncomms12978.

(13) Tran, T. T.; Bray, K.; Ford, M. J.; Toth, M.; Aharonovich, I. Quantum Emission from Hexagonal Boron Nitride Monolayers. *Nat. Nanotechnol.* **2016**, *11* (1), 37−41.

(14) Santori, C.; Fattal, D.; Yamamoto, Y. *Single-Photon Devices and Applications*; Wiley-VCH Verlag: Weinheim, 2010.

(15) O'Brien, J. L.; Furusawa, A.; Vučković, J. Photonic Quantum Technologies. *Nat. Photonics* **2009**, *3* (12), 687−695.

(16) Aharonovich, I.; Englund, D.; Toth, M. Solid-State Single-Photon Emitters. *Nat. Photonics* **2016**, *10* (10), 631−641.

(17) Pospischil, A.; Humer, M.; Furchi, M. M.; Bachmann, D.; Guider, R.; Fromherz, T.; Mueller, T. CMOS-Compatible Graphene Photodetector Covering All Optical Communication Bands. *Nat. Photonics* **2013**, *7* (11), 892.

(18) Knill, E.; Laflamme, R.; Milburn, G. J. A Scheme for Efficient Quantum Computation with Linear Optics. *Nature* **2001**, *409* (6816), 46−52.

(19) Aaronson, S.; Arkhipov, A. The Computational Complexity of Linear Optics. Proceedings from the *Forty-third Annual ACM Symposium on Theory of Computing* (STOC '11), San Jose, CA, June 6−8, 2011; ACM: New York, 2011; pp 333−342.

DOI: 10.1021/acs.nanolett.9b02640
Nano Lett. XXXX, XXX, XXX−XXX

(20) Empedocles, S. A.; Bawendi, M. G. Quantum-Confined Stark Effect in Single CdSe. *Science* **1997**, *278*, 2114.
(21) Reithmaier, J. P.; Sęk, G.; Löffler, A.; Hofmann, C.; Kuhn, S.; Reitzenstein, S.; Keldysh, L. V.; Kulakovskii, V. D.; Reinecke, T. L.; Forchel, A. Strong Coupling in a Single Quantum Dot−Semiconductor Microcavity System. *Nature* **2004**, *432* (7014), 197−200.
(22) Flagg, E.; Muller, A.; Polyakov, S.; Ling, A.; Migdall, A.; Solomon, G. Interference of Single Photons from Two Separate Semiconductor Quantum Dots. *Phys. Rev. Lett.* **2010**, *104* (13), 137401.
(23) Grosso, G.; Moon, H.; Lienhard, B.; Ali, S.; Efetov, D. K.; Furchi, M. M.; Jarillo-Herrero, P.; Ford, M. J.; Aharonovich, I.; Englund, D. Tunable and High-Purity Room Temperature Single-Photon Emission from Atomic Defects in Hexagonal Boron Nitride. *Nat. Commun.* **2017**, *8* (1), 705.
(24) Stevenson, R. M.; Young, R. J.; Atkinson, P.; Cooper, K.; Ritchie, D. A.; Shields, A. J. A Semiconductor Source of Triggered Entangled Photon Pairs. *Nature* **2006**, *439* (7073), 179−182.
(25) Chakraborty, C.; Goodfellow, K. M.; Dhara, S.; Yoshimura, A.; Meunier, V.; Vamivakas, A. N. Quantum-Confined Stark Effect of Individual Defects in a van Der Waals Heterostructure. *Nano Lett.* **2017**, *17* (4), 2253−2258.
(26) Tamarat, Ph.; Gaebel, T.; Rabeau, J. R.; Khan, M.; Greentree, A. D.; Wilson, H.; Hollenberg, L. C. L.; Prawer, S.; Hemmer, P.; Jelezko, F.; et al. Stark Shift Control of Single Optical Centers in Diamond. *Phys. Rev. Lett.* **2006**, *97* (8), No. 083002.
(27) Bassett, L. C.; Heremans, F. J.; Yale, C. G.; Buckley, B. B.; Awschalom, D. D. Electrical Tuning of Single Nitrogen-Vacancy Center Optical Transitions Enhanced by Photoinduced Fields. *Phys. Rev. Lett.* **2011**, *107* (26), 266403.
(28) Bernien, H.; Childress, L.; Robledo, L.; Markham, M.; Twitchen, D.; Hanson, R. Two-Photon Quantum Interference from Separate Nitrogen Vacancy Centers in Diamond. *Phys. Rev. Lett.* **2012**, *108* (4), 043604.
(29) Sipahigil, A.; Goldman, M. L.; Togan, E.; Chu, Y.; Markham, M.; Twitchen, D. J.; Zibrov, A. S.; Kubanek, A.; Lukin, M. D. Quantum Interference of Single Photons from Remote Nitrogen-Vacancy Centers in Diamond. *Phys. Rev. Lett.* **2012**, *108* (14), 143601.
(30) Lettow, R.; Rezus, Y. L. A.; Renn, A.; Zumofen, G.; Ikonen, E.; Götzinger, S.; Sandoghdar, V. Quantum Interference of Tunably Indistinguishable Photons from Remote Organic Molecules. *Phys. Rev. Lett.* **2010**, *104* (12), 123605.
(31) Noh, G.; Choi, D.; Kim, J.-H.; Im, D.-G.; Kim, Y.-H.; Seo, H.; Lee, J. Stark Tuning of Single-Photon Emitters in Hexagonal Boron Nitride. *Nano Lett.* **2018**, *18* (8), 4710−4715.
(32) Nikolay, N.; Mendelson, N.; Sadzak, N.; Böhm, F.; Tran, T. T.; Sontheimer, B.; Aharonovich, I.; Benson, O. Very Large and Reversible Stark-Shift Tuning of Single Emitters in Layered Hexagonal Boron Nitride. *Phys. Rev. Appl.* **2019**, *11* (4), No. 041001.
(33) Scavuzzo, A.; Mangel, S.; Park, J.-H.; Lee, S.; Loc Duong, D.; Strelow, C.; Mews, A.; Burghard, M.; Kern, K. Electrically Tunable Quantum Emitters in an Ultrathin Graphene−Hexagonal Boron Nitride van Der Waals Heterostructure. *Appl. Phys. Lett.* **2019**, *114* (6), No. 062104.
(34) Mendelson, N.; Xu, Z.-Q.; Tran, T. T.; Kianinia, M.; Scott, J.; Bradac, C.; Aharonovich, I.; Toth, M. Engineering and Tuning of Quantum Emitters in Few-Layer Hexagonal Boron Nitride. *ACS Nano* **2019**, *13* (3), 3132−3140.
(35) Müller, T.; Aharonovich, I.; Lombez, L.; Alaverdyan, Y.; Vamivakas, A. N.; Castelletto, S.; Jelezko, F.; Wrachtrup, J.; Prawer, S.; Atatüre, M. Wide-Range Electrical Tunability of Single-Photon Emission from Chromium-Based Colour Centres in Diamond. *New J. Phys.* **2011**, *13* (7), No. 075001.
(36) Geick, R.; Perry, C. H.; Rupprecht, G. Normal Modes in Hexagonal Boron Nitride. *Phys. Rev.* **1966**, *146* (2), 543−547.
(37) Brunel, Ch.; Tamarat, Ph.; Lounis, B.; Woehl, J. C.; Orrit, M. Stark Effect on Single Molecules of Dibenzanthanthrene in a Naphthalene Crystal and in a *n* -Hexadecane Shpol'skii Matrix. *J. Phys. Chem. A* **1999**, *103* (14), 2429−2434.

DOI: 10.1021/acs.nanolett.9b02640
Nano Lett. XXXX, XXX, XXX−XXX